HYDRODYNAMIC STABILITY IN ELECETROCHEMICAL CELLS

José Pontes – jopontes@metalmat.ufrj.br
Escola Politécnica/COPPE – Universidade Federal do Rio de Janeiro
P.O. Box 68505, Rio de Janeiro, RJ, 21941-972 Brasil
Norberto Mangiavacchi - norberto.mangiavacchi@gmail.com
Mechanical Engineering Department/GESAR Group, State University of Rio de Janeiro
R. São Francisco Xavier 524 20550-013 Rio de Janeiro, RJ, Brazil
Gustavo Rabello dos Anjos - gustavo.rabello@gmail.com
Mechanical Engineering Department/GESAR Group, State University of Rio de Janeiro
R. São Francisco Xavier 524 20550-013 Rio de Janeiro, RJ, Brazil

Abstract. *We consider the stability of rotating disk flow coupled, through the fluid viscosity, to the mass concentration field of a chemical species. This configuration refers to an electrochemical cell where the working electrode consists of an iron rotating rod, which is dissolved in the 1* $\mathbf{M}$ $\mathbf{H_2SO_4}$ *solution of the electrolyte. Polarization curves obtained in these cells present a current instability at the beginning of the region where the current is controlled by the mass transport. The instability appears at a certain value of the applied potential and is suppressed beyond another value. Dissolution of the electrode gives rise to a thin concentration boundary layer, due to a Schmidt number* $Sc = 2000$ *of the setup. This boundary layer, together with the potential applied to the electrode, leads to an increase in the fluid viscosity and to a decrease in the diffusion coefficient, both affecting the chemical species field. Since the current is proportional to the normal derivative of the species concentration at the interface, an instability of the coupled fields at sufficiently low Reynolds numbers may result in a current instability. In this work we review the main points related to the joint work conducted in the last ten years by the Metalurgy and Materials Engineering Dept./Program at the Federal University of Rio de Janeiro, togeteher with the Mechanical Engineering Graduate Program/GESAR Group, at the State University of Rio de Janeiro, related to the linear stability analisys of the hydrodynamic field close to the rotating disk electrode. in addition, we report the first steps towards a direct numerical simulation of the problem. The linear stability analysis shows that the coupling of the hydrodynamics to the cocentration field of a representative chemical species strongly reduces the stability of both. In addition, the coupling gives raise to a new unstable region of modes at even lower Reynolds numbers, of same order of those attained in the experimental setup. The amplitude of the concentration component of unstable modes in this new region is much larger than the amplitude of the hydrodynamic variables. Furthermore, the concentration unstable modes are confined to a boundary layer 20 times thinner than the hydrodynamic boundary layer. The combination of these two properties point to the existence of oscillations of the interfacial concentration gradient at levels sufficient high to induce detectable current oscillations. In addition, numerical experiments show that the new unstable regions collpase and the constant viscosity stability properties are recovered if a too high interfacial viscosity is attained, suggesting that this mechanism could be responsible for the collpase of the current oscillations. As a follow up of the stability analysis, a FEM-DNS code is under development at our group. The numerical solutions adopted are discussed and validation results of the proposed*

algorithm are presented.

Keywords: *Hydrodynamic Stability, Rotating Disk, Chemical Oscillations*

1. INTRODUCTION

Electrochemical cells using a rotating disk electrode are a widely used experimental tool in electrochemistry, due to the simplicity of the setup and the fact that the mass flux is independent of the radial position along the disk, at steady state conditions (LevichLevich (1962), 1962). The rate of transfer of ions close to the electrode is conveniently controlled through the angular velocity imposed to the electrode and this rate of transfer defines the maximum steady state current attained in an experiment. Polarization curves obtained in these cells present a current instability at the beginning of the region where the current is controlled by the mass transport. The instability appears at a certain value of the applied potential and is suppressed beyond another value (GeraldoGeraldo et al. (1998), 1998).

In the present paper we review the stability of the hydrodynamic field coupled to the transport of one relevant chemical species, originated from the dissolution of the iron electrode, presented by Mangiavacchi*et al.*. Coupling appears through a concentration dependent viscosity. Since the current is proportional to the normal derivative of the ions concentration at the electrode surface (BarciaBarcia et al. (1992), 1992) (see Sec. 3.2) a reduction on the critical Reynolds number to typical values found in experimental conditions could lead to a current instability. A phenomenological law is assumed, relating the fluid viscosity to the concentration of a representative chemical species, and the parameters of this law are estimated based on experimental electrochemical data. As a follow up of the stability analysis, a FEM-DNS code is under development at our group. The numerical solutions adopted are discussed and validation results of the proposed algorithm are presented.

2. GOVERNING EQUATIONS

The problem is governed by the continuity and the Navier-Stokes equations, coupled through the viscosity, to the transport equation of a relevant chemical species. These equations, written in the frame attached to the surface of the rotating disk read:

$$\operatorname{div} \mathbf{v} = 0 \tag{1}$$

$$\frac{D\mathbf{v}}{Dt} = -2\boldsymbol{\Omega} \times \mathbf{v} - \boldsymbol{\Omega} \times (\boldsymbol{\Omega} \times \mathbf{r}) - \frac{1}{\rho} \mathbf{grad}\, p + \frac{1}{\rho} \operatorname{div} \tau \tag{2}$$

$$\frac{D\mathcal{C}}{Dt} = \operatorname{div}(\mathcal{D}\, \mathbf{grad}\, \mathcal{C}) \tag{3}$$

where $\boldsymbol{\Omega}$ is the angular velocity of the rotating disk electrode, $\mathcal{C}$ and $\mathcal{D}$ are, respectively, the concentration and the diffusion coefficient of a representative chemical species and τ is the viscous stress tensor for a fluid with variable viscosity.

We rewrite the evolution equations in non-dimensional form. Variables having units of length or its reciprocal (radial and axial coordinates, perturbation wavenumber along the radial direction) are made non-dimensional with the length used to measure the thickness of the boundary layer, $(\nu_\infty/\Omega)^{1/2}$, where ν_∞ is the bulk viscosity of the fluid. Velocity components are divided by the local imposed azimuthal velocity $r_e\Omega$, pressure is divided by $\rho(r_e\Omega)^2$, viscosity is divided by the bulk viscosity, ν_∞, time and the eigenvalue of the linearized problem are made non-dimensional with the time required by a particle, turning with the azimuthal velocity $r_e\Omega$, to move a distance equal to the reference length, $(\nu_\infty/\Omega)^{1/2}$. Here, r_e is the dimensional coordinate along the radial direction at which the stability analysis is carried out. The non-dimensional

concentration of the chemical species is defined by:

$$C = \frac{\mathcal{C} - \mathcal{C}_\infty}{\mathcal{C}_S - \mathcal{C}_\infty} \tag{4}$$

where $\mathcal{C}_S$ and $\mathcal{C}_\infty$ are, respectively, the concentration of the chemical species at the electrode surface and in the bulk. We define also the Reynolds and the Schmidt numbers by the relations:

$$R = r_e \left(\frac{\Omega}{\nu_\infty} \right)^{1/2} \qquad \text{and} \qquad Sc = \frac{\mathcal{D}_\infty}{\nu_\infty} \tag{5}$$

At this point, we assume that the viscosity depends on the non-dimensional concentration of the chemical species according to:

$$\nu = \nu_\infty \exp(mC) \tag{6}$$

where m is a non-dimensional parameter depending on the electrochemical characteristics of the system (electrode material, type of electrolyte, applied potential), but not on the concentration of the chemical species. In particular, this parameter defines the interface viscosity, given by $\nu = \nu_\infty \exp(m)$. We also assume the Stokes-Einstein law, which postulates that the product of the diffusion coefficient by the viscosity is constant:

$$\mathcal{D}\nu = \mathcal{D}_\infty \, \nu_\infty \tag{7}$$

Equations (1–3) are rewritten as follows, in non-dimensional form:

$$\operatorname{div} \mathbf{v} = 0 \tag{8}$$

$$\frac{D\mathbf{v}}{Dt} = -2\,\mathbf{e}_z \times \mathbf{v} - \mathbf{e}_z \times (\mathbf{e}_z \times r\,\mathbf{e}_r) - \mathbf{grad}\, p + \frac{1}{R} \operatorname{div} \tau \tag{9}$$

$$\frac{DC}{Dt} = \frac{1}{R\,Sc} \operatorname{div}(\mathcal{D}\,\mathbf{grad}\, C) \tag{10}$$

A destabilizing potential of the coupling between the hydrodynamic and the chemical species fields can be seen in Eqs. (8–10): the Reynolds number in Eq. (10) is multiplied by the Schmidt number, which takes here the value $Sc = 2000$, typical for electrochemical cells.

3. THE BASE STATE

3.1 Base State Equations

The base state is the von Kármán similarity solution for a fluid with the viscosity depending on the concentration field, which is assumed to vary along the axial coordinate only.

$$\begin{pmatrix} \bar{v}_r \\ \bar{v}_\theta \\ \bar{v}_z \\ \bar{p} \\ \bar{\mathcal{C}} \end{pmatrix} = \begin{pmatrix} r\,\Omega\,F(z) \\ r\,\Omega\,G(z) \\ (\nu_\infty\,\Omega)^{1/2}\;H(z) \\ \rho\nu_\infty\Omega\,P(z) \\ \mathcal{C}_\infty + (\mathcal{C}_S - \mathcal{C}_\infty)\,C(z) \end{pmatrix} \tag{11}$$

All variables in Eq. (11) are dimensional, except the axial dependent profiles, F, G, H, C and the axial coordinate z. Boundary conditions for F, G, H and P are $F = G = H = P = 0$ at the disk surface $(z = 0)$, $F = H' = 0$ and $G' = -1$ as $z \longrightarrow \infty$. The non-dimensional concentration profile, C, varies from 1, at $z = 0$, to 0, as $z \longrightarrow \infty$.

Introducing Eq. (11) and the constitutive equations of the Newtonian stress tensor (dos Anjosdos Anjos et al. (2006a)) in Eqs. (1 – 3), together with Eqs. (6) and (7), we obtain the ordinary nonlinear system for the axial profiles F, G, H, P and C:

$$\begin{aligned} 2F + H' &= 0 && (12)\\ F^2 - (G+1)^2 + HF' - \nu F'' - \nu' F' &= 0 && (13)\\ 2F(G+1) + HG' - \nu G'' - \nu' G' &= 0 && (14)\\ P' + HH' - \nu H'' - 2\nu' H' &= 0 && (15)\\ Sc\, HC' - \frac{C''}{\nu} + \frac{\nu'}{\nu^2} C' &= 0 && (16) \end{aligned}$$

where prime denotes derivatives with respect to the non-dimensional axial coordinate z. The viscosity ν and its derivatives are written in non-dimensional form in the above equations, and:

$$\nu' = m \exp(mC)\, C'. \tag{17}$$

3.2 Evaluation of the Viscosity at the Electrode/Electrolyte Interface

Eqs. (12 – 16) are solved using the Newton method, in a staggered, uniform grid of points, with space derivatives represented by second order approximations. Solving these equations requires specification of two parameters: the bulk Schmidt number and the parameter m appearing in Eq. (6), which ultimately defines the electrolyte viscosity at the interface with the electrode. Though both questions will be addressed in a separate paper by the authors we briefly review the key points of the subject for the sake of completeness.

At this point, we assume that the limit current density at the interface is proportional to the concentration gradient of the relevant chemical species generated by the dissolution of the electrode. Ions migration due to the potential gradient is neglected. The current density is given by the relation (BarciaBarcia et al. (1992), 1992):

$$\frac{i}{n\mathcal{F}\dfrac{1}{Sc}\dfrac{1}{\nu_0/\nu_\infty}\left(\mathcal{C}_\infty - \mathcal{C}_s\right)\sqrt{\nu_\infty \Omega}} = \left.\frac{dC}{dz}\right|_{z=0} \tag{18}$$

where i is expressed in A/cm^2, n is the valence number of the chemical species $(n = 2)$, $\mathcal{F} = 96500\, C/mol$, is the Faraday constant, $\mathcal{C}_s = 2.0 \times 10^{-3} mol/cm^3$ is the dimensional concentration of the species at the electrode interface (saturated condition), $\mathcal{C}_\infty = 0\, mol/cm^3$ and ν_0 is the fluid viscosity at the interface. The limit current density obtained experimentally is $i = 0.8810\, A/cm^2$ at $900\, rpm$ (GeraldoGeraldo et al. (1998), 1998).

An initial value is specified for m, Eqs. (12 – 16) are solved. The ratio ν_0/ν_∞ is evaluated and the non-dimensional normal derivative of the concentration at the interface, $dC/dz|_{z=0}$, is obtained from the profiles. These figures are introduced in Eq. (18), leading to a value for the current density. The value initially specified for m is corrected and the procedure is repeated until convergence to the experimental value of i is reached. At convergence we obtain $\nu_0/\nu_\infty = 2.255$ $(m = \ln \nu/\nu_\infty)$.

3.3 Base State Profiles

The high Schmidt number leads to a concentration boundary layer much thinner than the hydrodynamic one. An estimation of the ratio between the thicknesses of the hydrodynamic (δ_h) and the concentration (δ_c) boundary layers can be made by using the relation $\delta_h/\delta_c \approx 2\, Sc^{1/3}$ proposed by LevichLevich (1962). Upon assuming $\delta_h = 6$ for the hydrodynamic boundary

layer we estimate $\delta_c = 0.24$, using the above relation. The profiles numerically obtained agree with this estimate.

The thin concentration boundary layer results in velocity profiles very close to the ones obtained for the constant viscosity case. In particular, we obtain $H = -0.88559$ far from the disk for the variable viscosity flow considered, a figure slightly different from the asymptotic value for the constant viscosity case, $H = -0.88447$. However, the derivatives of the velocity profiles are strongly affected inside the concentration boundary layer (Mangiavacchi *et al*, 2007).

4. STABILITY OF THE BASE STATE

4.1 Stability Equations

We turn now to the question of the stability of the base state with respect to small disturbances. The hydrodynamic and chemical fields are written as a sum of the base state plus a perturbation:

$$\left.\begin{array}{lllllllll} v_r & = & \bar{v}_r + \tilde{v}_r & & v_\theta & = & \bar{v}_\theta + \tilde{v}_\theta & & v_z & = & \bar{v}_r + \tilde{v}_z \\ p & = & \bar{p} + \tilde{p} & & \mathcal{C}_T & = & \bar{\mathcal{C}} + \tilde{\mathcal{C}} & & & & \end{array}\right\} \tag{19}$$

where the perturbation, in dimensional form, is given by:

$$\begin{pmatrix} \tilde{v}_r \\ \tilde{v}_\theta \\ \tilde{v}_z \\ \tilde{p} \\ \tilde{\mathcal{C}} \end{pmatrix} = \begin{pmatrix} r_e \Omega\, f \\ r_e \Omega\, g \\ r_e \Omega\, h \\ \rho \nu_\infty \Omega\, \pi \\ (\mathcal{C}_s - \mathcal{C}_\infty)\, c \end{pmatrix} \exp\left[i(\alpha r + \beta R\theta - \omega t)\right] + cc. \tag{20}$$

Here ω is a complex number, with $\Re(\omega)$ and $\Im(\omega)$ being, respectively, the frequency and the rate of growth of the perturbation. The functions f, g, h, π and c depend on the axial coordinate z and the parameters α and β are the components of the perturbation wave-vector along the radial and azimuthal directions. The base and the perturbation, given by Eqs. (11) and (20), are rewritten in non-dimensional form:

$$\begin{pmatrix} \bar{v}_r \\ \bar{v}_\theta \\ \bar{v}_z \\ \bar{p} \\ \bar{C} \end{pmatrix} = \begin{pmatrix} rF/R \\ rG/R \\ H/R \\ p/R^2 \\ C \end{pmatrix} \qquad \begin{pmatrix} \tilde{v}_r \\ \tilde{v}_\theta \\ \tilde{v}_z \\ \tilde{p} \\ \tilde{c} \end{pmatrix} = \begin{pmatrix} f \\ g \\ h \\ \pi \\ c \end{pmatrix} \exp\left[i(\alpha r + \beta R\theta - \omega t)\right] + cc \tag{21}$$

The base state and the perturbation variables are introduced in Eqs. (8 – 10) and nonlinear terms are dropped. Perturbation variables are not, strictly speaking, separable since the resulting equations for the profiles f, g, h, π and c still contain the radial coordinate r. In order to overcome the problem it is necessary to make the *parallel flow* assumption, where it is assumed that variations of the above profiles are small as far as $\Delta r/r \ll 1$. This approximation holds whenever the stability analysis is carried sufficiently far from $r = 0$. If variations of the profiles with r are small, this coordinate can be assumed as constant. The non-dimensional constant r is the Reynolds number at which the stability analysis is carried. This is the parallel flow hypothesis. Adoption of this hypothesis in rotating disk flowMalik et al. (1981); Wilkinson & Malik (1985); Lingwood (1995), is made by replacing r by R.

To conclude, terms of order R^{-2} are dropped, leading to a generalized complex non-symmetric eigenvalue-eigenfunction problem in the form:

$$\begin{pmatrix} A_{11} & A_{12} & A_{13} \\ A_{21} & A_{22} & A_{23} \\ A_{31} & & A_{33} \end{pmatrix} \begin{pmatrix} h \\ \eta \\ c \end{pmatrix} = \omega R \begin{pmatrix} B_{11} & & \\ & B_{22} & \\ & & B_{33} \end{pmatrix} \begin{pmatrix} h \\ \eta \\ c \end{pmatrix} \tag{22}$$

where $\eta = \alpha g - \beta f$, missing elements in the matrices are zero and the operators A_{ij} and B_{ij} are given by:

$$
\begin{aligned}
A_{11} &= a_{114}D^4 + a_{113}D^3 + a_{112}D^2 + a_{111}D + a_{110} \\
A_{12} &= a_{121}D + a_{120} \\
A_{13} &= a_{132}D^2 + a_{131}D + a_{130} \\
A_{21} &= a_{211}D + a_{210} \\
A_{22} &= a_{222}D^2 + a_{221}D + a_{220} \\
A_{23} &= a_{231}D + a_{230} \\
A_{31} &= a_{310} \\
A_{33} &= a_{332}D^2 + a_{331}D + a_{330}
\end{aligned}
$$

$$
B_{11} = D^2 - \bar{\lambda}^2 \qquad B_{22} = 1 \qquad B_{33} = iSc
$$

with $D^n = d^n/dz^n$ and $\lambda^2 = \alpha^2 + \beta^2$. By defining $\bar{\alpha} = \alpha - i/R$ and $\bar{\lambda}^2 = \alpha\bar{\alpha} + \beta^2$.

4.2 Stationary Neutral Curves

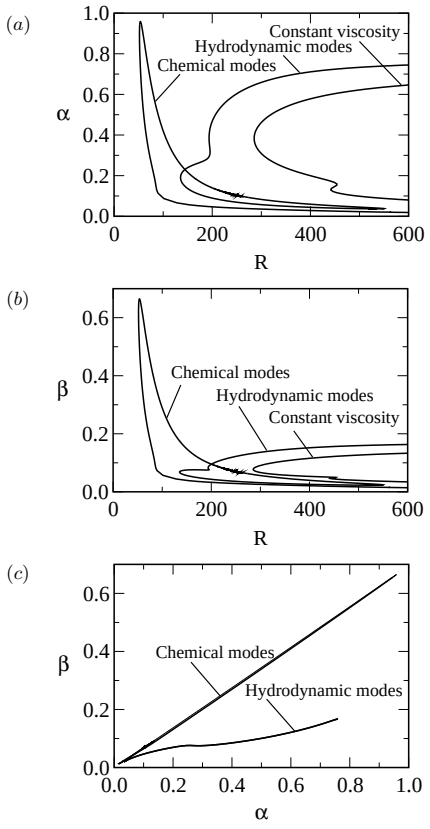

Figure 1: The neutral stability curves of stationary perturbations ($\Re(\omega) = 0$), in the $R \times \alpha$ (a), $R \times \beta$ (b) and $\alpha \times \beta$ (c) planes.

The neutral stability curves for stationary disturbances ($\Re(\omega) = 0$), obtained by solving the eigenvalue-eigenfunction problem for $Sc = 2000$ and $\nu_0/\nu_\infty = 2.255$, are presented in Fig. 1. This figure shows that the coupling of the mass concentration to the hydrodynamic field affects the stability properties of the coupled fields, by enlarging the unstable region to a wider range of wave-numbers and to a critical Reynolds number of order of 50% of the critical wavenumber of constant viscosity fluids.

Fig. (1) shows also the existence of a new family of much more unstable modes. We refer to these new modes as *chemical* and to modes belonging to the former family as *hydrodynamic*.

The new critical Reynolds number is now associated to modes in the border of the unstable region of chemical modes. The critical Reynolds number for stationary disturbances is $R = 52.3$, a number significantly smaller than 285.36, the critical value for constant viscosity fluids (Malik (1986), 1986).

We point out that the critical Reynolds number obtained is within the range of values attained in the experimental setup by GeraldoGeraldo et al. (1998) (1998). For instance, at $900\,rpm$, the Reynolds number based on the external radius of the electrode insulation ($r = 5 \times 10^{-3}m$ and $\nu_\infty = 1 \times 10^{-6}m^2s^{-1}$) is 48.54.

4.3 Growth Rate of Unstable Perturbations and Marginally Stable Eigenmodes

The enlarged unstable hydrodynamic region suggests that modes inside this region might possibly have larger growth rates (ω_i) than unstable modes of constant viscosity fluids. Similarly, we could expect that the narrow region of unstable chemical modes could not allow for the existence of modes with large growth rates. This is the case, indeed. Figure (2) shows neutral

and level curves evaluated for positive rates of growth for fluids with constant viscosity (a) and for the unstable region of hydrodynamic and chemical modes (b and c, respectively).

An analysis of Fig. (2) shows that growth rates of chemical modes are more than one order of magnitude smaller than those of hydrodynamic modes. Growth rates are particularly small close to the electrode axis. As the point of analysis moves to larger distances from the electrode axis, the unstable region of chemical modes becomes narrower and limited to small wave-numbers, but higher growth rate are found. Nevertheless, the growth rates of chemical modes stay always one order of magnitude smaller than the one of hydrodynamic modes. Finally, a comparison between growth rates of hydrodynamic and constant viscosity unstable modes (Fig. $2a$ and b) shows an increase of order of 30% in the former. We address now the question of whether unstable chemical modes with critical Reynolds numbers on the order of 60 and growth rates 20 times smaller than typical unstable hydrodynamic modes could give raise to detectable current oscillations.

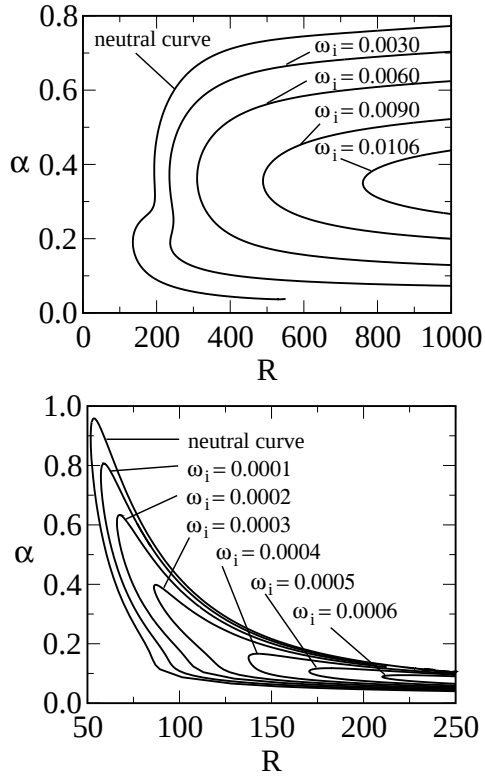

Figure 2: Neutral and level curves with positive growth rates (ω_i) of hydrodynamic (b) and chemical modes (c) of the coupled case, in the $R \times \alpha$ planes.

In order to answer the question we mention that the amplitude of instabilities emerging from a Hopf bifurcation increase with the the instability growth rate. Weakly nonlinear theory shows that the amplitude of unstable modes associated to complex eigenvalues saturates at levels proportional to the square root of the growth rate. A second factor affecting the amplitude of the current instability is the relative amplitude of the concentration component c of the eigenmodes, with respect to the amplitude of the hydrodynamic components, h and η. A third factor is the value of $dc/dz|_{z=0}$.

Fig. (3) shows marginally stable modes on two points at the neutral curve of the chemical region. An analysis Fig. (3) shows that the amplitude of the c component of the modes in the chemical region is always 10 to 20 times larger than the amplitude of h and η. The eigenfunction is dominated by the chemical component c. The chemical component c stays confined to a thin layer with thickness $\delta_c \approx 0.3$, a characteristic length 20 times smaller than the length scale of the hydrodynamic variables h and η. Since $dc/dz|_{z=0}$ is of order of δ_c^{-1}, very high values of this derivative are expected;

Summing up, the low growth rate of the perturbation is balanced by the high value taken by the chemical component c and by its normal derivative at the electrode surface. The modes in the new region are dominated by the concentration component of the eigenfunction, justifying thus the name of *chemical modes*. These facts indicate that the concentration fluctuations in the chemical region are sufficiently large to drive the current instability found in experimental conditions.

Numerical experiments conducted with different viscosity profiles show that the minimum value of the critical Reynolds number is not attained for $\nu_0/\nu_\infty = 2.255$, nor is the new unstable

region, associated to this case, the largest one. Cases with $\nu_0/\nu_\infty = 1.8$ and 1.5 show a larger new region of chemical modes, with a critical Reynolds very close to the one associated o the case with $\nu_0/\nu_\infty = 2.255$. By further reducing the ν_0/ν_∞, the new unstable region of chemical modes moves to higher Reynolds numbers as $\nu_0/\nu_\infty \longrightarrow 1$ and eventually disappears, as the condition of constant viscosity fluid is reached. The neutral stability curve for constant viscosity fluids is recovered.

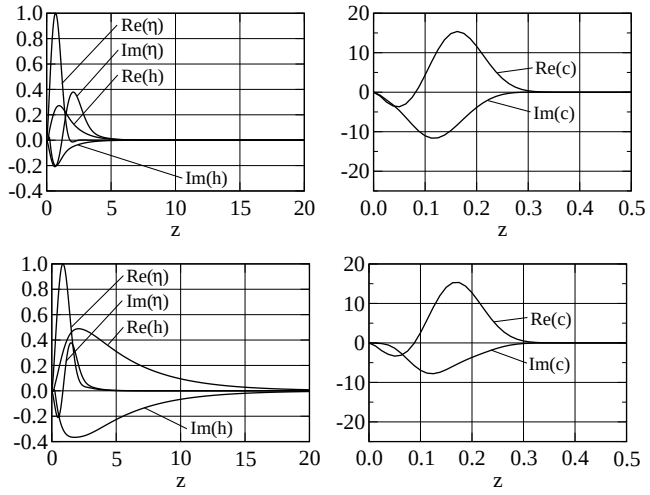

Figure 3: Real and imaginary parts of three modes on the neutral curve of the chemical region, at the points $R = 64.369$, $\alpha = 0.81250$, $\beta = 0.56278$ (first row) and $R = 156.99$, $\alpha = 0.20124$, $\beta = 0.13767$ (second row). The eigenfunction is dominated by the chemical component c, which attains values more than 20 times larger than those associated to the hydrodynamic variables h and η. The chemical component c is confined to a thin layer close to the interface, leading to short range variations and to high values of $dc/dz|_{z=0}$.

Upon increasing the value of ν_0/ν_∞ beyond the value 2.255 the new unstable region also collapses and the neutral curve of hydrodynamic modes moves towards the neutral curve of constant viscosity fluids. This result suggests that a progressive increase of the interfacial viscosity and the high Schmidt number leads to an *in facto* discontinuity of the hydrodynamic field, with a thin viscous and stable region at the interface and a restored constant viscosity hydrodynamic boundary layer.

5. THE FEM-DNS APPROACH

Finite Element Methods became a powerfull tool for the analysis of fluid problems during the eighties, thanks to the works of T. J. R. Hughes, O. Pironneau and J. Donea, among others. The possibility of reusing written parts of codes and the adaptability to complex geometry problems contributed to the diffusion of the method in the community involved with fluid flow problems. When dealing with such problems we face two major issues related to the pressure-velocity coupling and to the solutions adopted for the convective term. Galerkin methods are currently used but stability problems limit the use of the method when large time intervals and/or large Reynolds numbers are involved. A Semi-Lagrangean approach was addopted in the code presently under devlopment in our group, solving the two problems pointed above. Semi-Lagrangean methods have been successefully employed in climatic numerical simulations Durran (1998), where large time-steps are crucial for efficient numerical simulations. Though being less used in other fluid flow problems, recent works demonstrate the effectiveness of the method dos Anjos et al. (2006a) and dos Anjos et al. (2006b), particularly when large Reynolds numbers are involved. The strict use of Lagrangean coordinates leads to unstable numerical schemes, since the trajectories rapidly become chaotic even for laminar flows. A Semi-Lagrangean approach avoids the problem, by reinitializing the Lagrangean coordinate system after each time step. The method is explicit since information from the preceding time step is required. However the information from the previous time step does not come necessarily form a grid point and an interpolation between neighbour nodes is required . The precision of the method depends on the degree of the interpolating polynomial.

A large choice of elements is available for the FEM method. Elements are classified by the geometry (tetrahedral, hexahedrals or prismatic), by the interpolation scheme, which may

use linear, quadratic, bilinear, cubic, etc., polynomials. Isoparametric elements are particularly suitable for use in problems with curved boundaries.

Restrictions on the choice of the element type appear in fluid flow problems, where variables are coupled. This restriction is usually known as the Babuska-Brezzi condition and restricts the elements choice to those satisfying this condtion and, consequently, the required stability properties. The Babuska-Brezi condition was addressed by several authors Cuvelier et al. (1986), Zienkiewicz & Taylor (2000) and Oden & Carey (1984). Elements not satisfying the Babuska-Brezzi may be used in some cases, provided that the Galerkin method is not adopted simultaneously. Two types of elements were employed in the present work, namely linear tetrahedrons and the *mini* tetrahedron. Simpler implementations are achieved with the former for three-dimensional problems and were adopted for the discretization of the transport equation of the representative chemical species. The *mini* tetrahedron belongs to the *Taylor-Hood* family of elements and combines the linear element with and additional internal node at the element centroid and leading to five nodes per element. This element satisfies the Babuska-Brezzi condition.

Following the spatial discretizations a linear system of algebraic equations is obtained. Several methods can be used for solving the system and attention is given to limit the computational component cost CPU time and memory storage requirements. Coupled methods look for solving the complete linear system at each time step. The strong pressure-velocity coupling and the non-linearities of the convective term result in computational inefficiencies if one tries a direct solution of the complete linear system, including the transport equation of the representative chemical species. Uncoupled solutions have thus, been envisaged to overcome the problem. A short description is given below, of a method based on the block LU factorization method, used in this work:

$$\begin{bmatrix} \mathbf{B} & -\Delta t\mathbf{G} \\ \mathbf{D} & 0 \end{bmatrix} \cdot \begin{bmatrix} ^{n+1} \\ p^{n+1} \end{bmatrix} = \begin{bmatrix} r^n \\ 0 \end{bmatrix} + \begin{bmatrix} \mathbf{bc_1} \\ \mathbf{bc_2} \end{bmatrix}$$

The above linear system, where $B = 1/\Delta t\, M + 1/\Delta Re\, K$ shows the typical structure resulting from the spatial discretization of the Navier-Stokes equations. Pressure is subsequently decoupled from the velocity trough the use of the projection method, leading to:

$$\begin{bmatrix} \mathbf{B} & 0 \\ \mathbf{D} & \Delta t\mathbf{D}\mathbf{B^{-1}}\mathbf{G} \end{bmatrix} \cdot \begin{bmatrix} \mathbf{I} & -\Delta t\mathbf{B^{-1}}\mathbf{G} \\ 0 & \mathbf{I} \end{bmatrix} \cdot \begin{bmatrix} ^{n+1} \\ p^{n+1} \end{bmatrix} = \begin{bmatrix} r^n \\ 0 \end{bmatrix} + \begin{bmatrix} \mathbf{bc_1} \\ \mathbf{bc_2} \end{bmatrix}$$

Solving the above equation in blocks leads to a highly efficient method, with acceptable computational costs and lower memory requirements, when compared to coupled methods.

Fig. 4 shows results of the FEM simulations: the velocity profiles for constant viscosity, on the left, and for variable viscosity, on the right. The results agree with the analytical von Kármán solution. The boundary layer for the variable viscosity is thicker than the constant viscosity case, and presents an additional inflection point, increasing thus the unstability of the profile.

The FEM code is now validated and will be employed for the simulation of the nonlinear evolution of the most unstable modes found in the linear analysis.

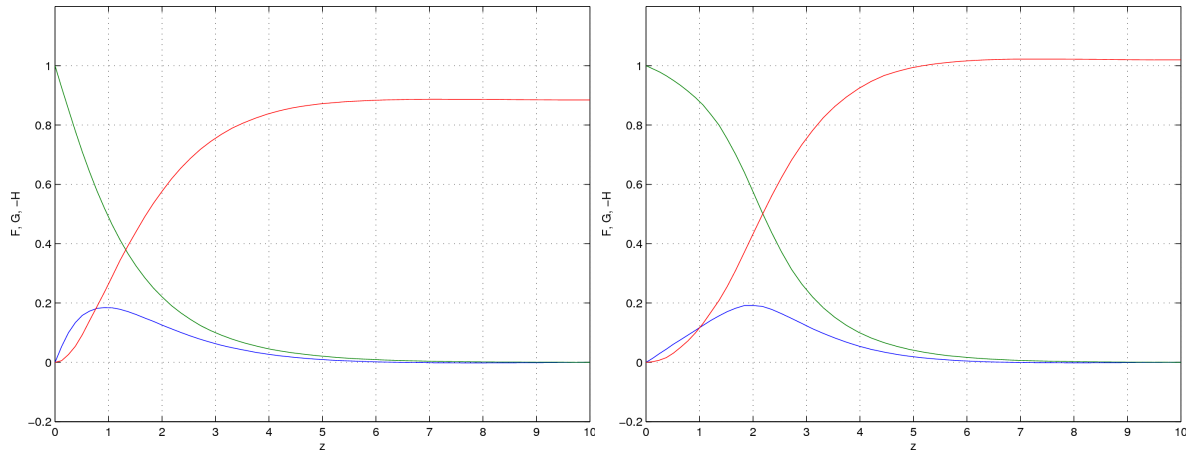

Figure 4: Velocity profiles obtained from the FEM simulation of the disk flow for constant viscosity fluids (left) and stratified viscosity (right).

REFERENCES

Barcia, O., Mattos, O., & Tribollet, B., 1992. Anodic dissolution of iron in acid sulfate under mass transport control. *J. Eletrochem. Soc.*, vol. 139, pp. 446–453.

Cuvelier, C., Segal, A., & van Steenhoven, A. A., 1986. *Finite Element Method and Navier-Stokes Equations*. Dordrecht, Holland.

dos Anjos, G., Mangiavacchi, N., Pontes, J., & Botelho, C., 2006a. Modelagem numérica de escoamentos acoplados ao transporte de uma espécie química pelo método dos elementos finitos. ENCIT 2006 - Congresso Brasileiro de Ciências Térmicas e Engenharia. Curitiba - PR.

dos Anjos, G., Mangiavacchi, N., Pontes, J., & Botelho, C., 2006b. Simulação numérica das equações de saint-venant utilizando o método dos elementos finitos. 16 POSMEC - Simpósio de Pós-Graduação em Engenharia Mecânica. Uberlândia - MG.

Durran, D., 1998. *Numerical Methods for Waves Equations in Geophysical Fluid Dynamics*. Springer-Verlag, 1a. edition.

Geraldo, A. B., Barcia, O. E., Mattos, O., Huet, F., & Tribollet, B., 1998. New results concerning the oscillations observed for the system iron-sulphuric acid. *Electrochim. Acta*, vol. 44, pp. 455–465.

Levich, V., 1962. *Physicochemical Hydrodynamics*. Prentice Hall.

Lingwood, R., 1995. Absolute instability of the boundary layer on a rotating disk. *Journal of Fluid Mechanics*, vol. 299, pp. 17–33.

Malik, M., 1986. The neutral curve for stationary disturbances in rotating-disk flow. *Journal of Fluid Mechanics*, vol. 164, pp. 275–287.

Malik, M., Wilkinson, & Orzag, S., 1981. Instability and transition in a rotating disk. *AIAA J.*, vol. 19-9, pp. 1131–1138.

Oden, J. T. & Carey, G., 1984. *Finite Elements: Mathematical Aspects*. Prentice-Hall, vol. iv edition.

Wilkinson, S. & Malik, M., 1985. Stability experiments in the flow over a rotating disk. *Journal of Fluid Mechanics*, vol. 23, pp. 588.

Zienkiewicz, O. C. & Taylor, R. L., 2000. *The Finite Element Method for Fluids Dynamics*. Wiley John and Sons, 5th edition edition.